Crystal structure and magnetic properties of potassium erbium double tungstate $KEr(WO_4)_2$

2007 J. Phys.: Condens. Matter 19 056206

(http://iopscience.iop.org/0953-8984/19/5/056206)

INSTITUTE OF PHYSICS PUBLISHING JOURNAL OF PHYSICS: CONDENSED MATTER

J. Phys.: Condens. Matter **19** (2007) 056206 (16pp) doi:10.1088/0953-8984/19/5/056206

Crystal structure and magnetic properties of potassium erbium double tungstate $KEr(WO_4)_2$

M T Borowiec[1], V P Dyakonov[1,2], K Woźniak[3], Ł Dobrzycki[3], M Berkowski[1], E E Zubov[2], E Michalski[4], A Szewczyk[1], M U Gutowska[1], T Zayarnyuk[1] and H Szymczak[1]

[1] Institute of Physics, Polish Academy of Sciences, al. Lotników 32/46, 02 668 Warsaw, Poland
[2] A A Galkin Physico-Technical Institute, 340114 Donetsk, Ukraine
[3] Chemistry Department, Warsaw University, 02 093 Warsaw, Poland
[4] Institute of Applied Physics, Military University of Technology, 00-908 Warsaw, Poland

E-mail: borow@ifpan.edu.pl

Received 1 August 2006, in final form 28 December 2006
Published 17 January 2007
Online at stacks.iop.org/JPhysCM/19/056206

Abstract

Results of structural, magnetic and specific heat investigations of the potassium erbium double tungstate, $KEr(WO_4)_2$, are presented. Potassium erbium double-tungstate $KEr(WO_4)_2$ single crystals have been grown by the top-seeded solution growth method (TSSG) and modified Czochralski techniques. It crystallizes in the monoclinic crystal structure ($C2/c$ space group). The unit cell contains four formula units and is described by parameters $a = 10.615(2)$ Å, $b = 10.316(2)$ Å, $c = 7.534(2)$ Å, $\beta = 130.73(3)^\circ$. From the x-ray diffraction measurements the fractional atomic coordinates, displacement parameters and interatomic distances have been determined.

The specific heat $C(T)$ of the $KEr(WO_4)_2$ crystal has been measured over a temperature range of 0.6–300 K. The susceptibility has been studied at $T = 0.25$–4.0 K. The magnetic phase transition was observed at a temperature of 0.48 K. The magnetization has been measured in the temperature region from 4.2 to 60 K and in magnetic field up to 1.6 T. A strong anisotropy of magnetic properties was found. The temperature and field dependences of susceptibility and magnetization data were used for both elucidation of character of the magnetic ordering and calculation of the exchange and dipole–dipole interaction energies as well as for determination of the possible magnetic structure of $KEr(WO_4)_2$.

1. Introduction

Alkaline rare earth double tungstates have been actively studied since the beginning of the 1970s. These crystals with third-order nonlinear optical properties can be used for

multifrequency solid-state laser applications [1]. They are characterized by a strong magnetic anisotropy, a low local symmetry, low-dimensional magnetic structure and strong spin–lattice coupling [2–4]. These properties are not usually observed in crystals of higher symmetry.

Physical properties of monoclinic double tungstates with a general formula $MRE(WO_4)_2$, where M and RE are alkaline and rare earth ions, respectively, result from competition between spin–spin, electron–phonon and magnetoelastic interactions, which determine the variety of magnetic, electron and crystallographic structures in such systems.

Many of the unusual physical properties of RE double tungstates are determined by the partly filled 4f-electron shell of the rare earth ions. It is known that, due to screening by outer electrons, the influence of crystal field on f electrons is much smaller than on d electrons. Nevertheless, under the influence of the crystal field of low symmetry the lowest energy levels are doublets for the RE ions with an odd number of electrons and singlets for the RE ions with an even number of electrons [3–7].

One of the unusual behaviours of these materials, despite their low symmetry, is a manifestation of the cooperative Jahn–Teller effect (CJTE), which was not predicted by the theory [8]. The CJTE is caused by both the existence of quasi-degenerate ground-state energy levels and a strong influence of the spin–phonon interaction. To date, this effect has been observed in dysprosium and holmium double tungstates $MRE(WO_4)_2$, where M = K, Rb, RE = Ho^{3+}, Dy^{3+} [7, 9–15].

Simultaneously with the structural phase transitions, the antiferromagnetic phase transitions with the Néel temperatures 0.6 K for $KDy(WO_4)_2$ and 0.82 K for $RbDy(WO_4)_2$ were observed in these crystals [15–17].

The low temperatures of magnetic phase transitions (MPTs) are indicative of the weak exchange interactions.

Since the ionic radii of different rare earth ions have close values, almost all RE ions can be introduced into crystals without change of their crystal symmetry and without significant change of the crystal lattice parameters. For almost all RE ions, doped to double tungstates, the laser radiation was observed [18–22]. In crystals in which mutually competing exchange, dipole–dipole and Jahn–Teller (electron–phonon) interactions exist one can expect an unusual magnetic behaviour, and it is difficult to predict the character of the magnetic ordering.

In this paper we present the results of our study of potassium erbium double-tungstate $KEr(WO_4)_2$ single crystals. Studies of magnetic properties of the $KEr(WO_4)_2$ crystal are of interest because of the interrelation between magnetic and elastic ordering realized in these magneto-elastic effect [2, 17].

We are going to present the results of the x-ray structural, specific heat, susceptibility and magnetization measurements of potassium erbium double-tungstate $KEr(WO_4)_2$ single crystals. The crystal structure, peculiarities of magnetic ordering and character of spin–spin interactions in this low-dimensional magnet will be established. The peculiarities of magnetic ordering will be discussed using the 2D Ising, 3D Ising and XY models and parameters of the exchange interaction will be estimated. An attempt to describe the magnetic structure of $KEr(WO_4)_2$ will be presented.

2. Experimental details

The specific heat investigations have been carried out using a computer controlled quasi-adiabatic calorimeter over a temperature range from 0.6 to 15 K. For these experiments a ^{3}He cryostat was used. Two RuO_2 thermometers of small size were applied to determine the sample temperature. The sample was mounted on a sapphire plate using the vacuum grease 'Apiezon N'. Both the amount of vacuum grease used and the area contact between sample and sapphire

plate were kept to a minimum in order to avoid strain in the sample that could adversely influence the magnetic phase transition properties. A small-size heater on the polyethylene film was used to supply heat pulses using a four-wire constant-power technique with precisely timed pulses. Small heat pulses were used. Near the MPT this causes a typical increase of the temperature by 0.001 or 0.0015 K.

Additional specific heat investigations were performed using a specific heat option of the Quantum Design physical property measurement system, in which a relaxation method is applied to determine heat capacity. In this apparatus, the mass of the sample can range from 2 to 500 mg and the specific heat can be measured over the temperature range from 1.9 to 385 K, in the external magnetic field up to 9 T.

The magnetization measurements have been carried out, using the vibrating sample magnetometer (PAR model 450), over the temperature range from 4.2 to 60 K, in magnetic field up to 1.6 T. The field was applied in the *ab*, *bc* and *ac* planes. The samples had the shape of cylinders with diameters and lengths approximately equal to 1.5 and 4 mm, respectively. The rotary axis of the cylinder coincided with one of the crystallographic axes (**a**, **b**, **c**). The angular dependence of the magnetization allows us to determine the magnetic **x**, **y**, **z** axes, among which the **y** axis coincides with the crystalline **b** axis and the **x** and **z** axes lie in the *ac* plane. The magnetic **z** and **x** axes correspond to the directions of maximal and minimal values of magnetization in the *ac* plane, respectively.

The differential magnetic susceptibility, $\chi = \mathrm{d}M/\mathrm{d}H$, was measured by the ac induction technique with measuring ac field of amplitude $H = 2$ Oe and frequency $f = 300$ Hz. The sample had a cylindrical form (2 mm in diameter and 6 mm in length). The measurements have been performed in a ^{3}He–^{4}He dilution refrigerator at temperatures of 0.25–4 K.

3. Structural studies

Single crystals of $KEr(WO_4)_2$ were grown by the top seeded solution growth (TSSG) method, using $K_2W_2O_7$, the eutectic composition of the K_2O–WO_3 system, as solvent. This solvent is convenient as flux, because it does not introduce additional ions to the solution. The low melting temperature, viscosity, relatively low evaporation and good solubility allow stable growth of the double-tungstate crystal. A solution composition of 25% of solute and 75% of solvent was chosen. The starting components, K_2CO_3 with 5N, WO_3 and Er_2O_3 with 4N purity, were mixed in a cylindrical platinum crucible 60 mm high and 40 mm in diameter. The crucible was placed inside the lower heating zone of the two-zone resistance furnace. The two-zone construction of the furnace allowed shaping of the temperature gradients in the crystallization region [23, 24]. Very low temperature gradients (about 6 °C cm^{-1}) have been used during crystal growth. Homogenization of the solutions was achieved by maintaining components at about 40 °C above the expected saturation temperature for 24 h. Growing crystals were rotated at 50 rpm and during the first 3 days were pulled up at a rate of 1.5 mm/day. Next crystal growth takes place only under the solution level on (111), (110), (201), (100) and (010) type facets. The temperature was lowered at the rate of 0.1–0.3 °C h^{-1}. The used range of growing temperature was 920–860 °C. After the growth process crystals were cooled down to room temperature with the rate of 30 °C h^{-1}. The first $KEr(WO_4)_2$ crystals were obtained by the TSSG method on platinum wire. These as-grown crystals with orientation along the ⟨001⟩ direction were used as seeds in the next crystal growth processes.

X-ray diffraction measurements were performed for a prismatic $KEr(WO_4)_2$ single crystal with the dimensions $0.25 \times 0.19 \times 0.16$ mm^3, using a Kuma KM4CCD four-circle κ-axis diffractometer with graphite-monochromated Mo Kα radiation, applying the omega scan technique. The crystal was positioned 65 mm from the KM4CCD camera. Collection of data

Table 1. Crystal data and structure refinement for $KEr(WO_4)_2$.

Empirical formula	$ErKO_8W_2$
Formula weight	702.06
Temperature	293(2) K
Wavelength	0.710 73 Å
Crystal system, space group	Monoclinic, $C2/c$
Unit-cell dimensions	$a = 10.615(2)$ Å, $b = 10.316(2)$ Å, $\beta = 130.73(3)°$, $c = 7.5343(15)$ Å,
Volume	625.3(2) Å^3
Z, calculated density	4, 7.458 mg cm^{-3}
Absorption coefficient	50.673 mm^{-1}
$F(000)$	1196
Crystal size	0.25 mm × 0.19 mm × 0.16 mm
Theta range for data collection	3.35°–32.49°
Limiting indices	$-15 \leqslant h \leqslant 16$, $-15 \leqslant k \leqslant 15$, $-11 \leqslant l \leqslant 11$
Reflections collected / unique	6652/1128[R(int) = 0.0850]
Completeness to theta = 32.49	99.2%
Absorption correction	Analytical
Transmission factors	$T_{min} = 0.003\,76$, $T_{max} = 0.065\,16$
Refinement method	Full-matrix least squares on F^2
Data/restraints/parameters	1128/0/57
Goodness-of-fit on F^2	1.112
Final R indices [$I > 2$sigma(I)]	$R1 = 0.0288$, $wR2 = 0.0731$ for 1080 reflections
R indices (all data)	$R1 = 0.0307$, $wR2 = 0.0745$
Extinction coefficient	0.0041(2)
Largest diff. peak and hole	3.396 and −1.782 e Å^{-3}

for the $KEr(WO_4)_2$ sample was performed with accelerating voltage reduced to 34.2 kV to eliminate the evident '$\lambda/2$ contamination' effect [25]. The data were corrected for Lorentz and polarization effects. Analytical absorption correction was done applying a shape optimization procedure based on reflections 20 times higher than their errors. Data reduction and analysis were carried out using the Kuma diffraction program package.

The data were collected for the 2Θ range from 8° to 100° with 1° intervals. The unit-cell parameters were determined based on 7700 reflections, and the structure determination was based on reflections collected up to 2Θ equal to 65°.

The structure was solved by direct methods [26] and refined using SHELXL [27]. The refinement was based on F^2 for all reflections except those for which F^2 reached large negative values. Scattering factors were taken from tables 6.1.1.4 and 4.2.4.2 of [28].

Crystal data regarding the $KEr(WO_4)_2$ structure are given in table 1 together with the refinement details. Fractional atomic coordinates and anisotropic displacement parameters are given in tables 2 and 3, respectively. The coordination figures of W, Er and K cations are shown in figures 1(a) and (b) [29].

According to table 2, K and Er ions occupy special positions (4e according to Wyckoff notation in $C2/c$ space group), while W1 cation occupies a general position although its y coordinate is very close to $1/2$. This location influences thermal motions (table 3) of this atom—the off-diagonal anisotropic displacement parameters (ADPs) are almost equal to zero (within the level of errors: see $U(23)$, $U(12)$, respectively).

There are three kinds of polyhedra in the $KEr(WO_4)_2$ structure, depending on the central cation, namely, octahedron, dodecahedron and icosahedron around, respectively, W, Er and K ions (figure 1). Because of the low symmetry of particular sites in this structure, each

Table 2. Fractional atomic coordinates and equivalent isotropic displacement parameters ($Å^2 \times 10^3$).

	Wyckoff position	x	y	z	U(eq)
Er(1)	4e	1.0000	0.7718(1)	0.7500	9(1)
W(1)	8f	0.8035(1)	0.5000(1)	0.7642(1)	8(1)
K(1)	4e	1.0000	0.7990(2)	0.2500	16(1)
O(1)	8f	0.9766(5)	0.3914(4)	1.0308(8)	11(1)
O(2)	8f	0.8108(5)	0.4246(5)	0.5596(8)	11(1)
O(3)	8f	0.6262(5)	0.4193(5)	0.6885(8)	14(1)
O(4)	8f	0.7242(6)	0.6584(4)	0.6258(8)	13(1)

Table 3. Anisotropic displacement parameters (ADP) ($Å^2 \times 10^3$).

	$U(11)$	$U(22)$	$U(33)$	$U(23)$	$U(13)$	$U(12)$
Er(1)	10(1)	8(1)	8(1)	0	5(1)	0
W(1)	7(1)	8(1)	7(1)	1(1)	4(1)	0(1)
K(1)	14(1)	19(1)	15(1)	0	9(1)	0
O(1)	9(2)	11(2)	12(2)	0(2)	7(2)	−2(1)
O(2)	12(2)	10(2)	12(2)	1(2)	8(2)	0(1)
O(3)	11(2)	15(2)	14(2)	3(2)	7(2)	0(1)
O(4)	15(2)	7(2)	11(2)	0(1)	6(2)	0(1)

polyhedron is distorted. There are three shorter W–O distances (about 1.8 Å), two distances close to 2 Å and one longer than 2.3 Å. Distances between erbium ions and their oxygen ligands vary from 2.26 to 2.69 Å, and for K the distances vary from 2.76 to 3.36 Å.

The unit-cell parameters obtained (table 1) are $a = 10.615(2)$ Å, $b = 10.316(2)$ Å, $c = 7.534(2)$ Å, $\beta = 130.73(3)°$, with $Z = 4$ and the space group $C2/c$. In order to simplify the calculations below we chose an equivalent but nonconventional crystallographic unit cell ($a_I = 7.534(2)$ Å, $b_I = 10.316(2)$ Å, $c_I = 8.058(5)$ Å, $\beta_I = 94.382°$, $I2/a$, $Z = 4$), which was obtained by using the following system of equations: $\mathbf{c_I} = -(\mathbf{a_C} + \mathbf{c_C})$, $\mathbf{b_I} = \mathbf{b_C}$, $\mathbf{a_I} = \mathbf{c_C}$ [30], where **C** and **I** indices correspond to the space groups $C2/c$ and $I2/a$, respectively.

4. Magnetic studies

4.1. Energy spectrum of Er^{3+} ion

The Er^{3+} ion with its electron configuration $4f^{11}$ has the $^4I_{15/2}$ ground multiplet (spin $S = 3/2$, $\Delta E =$ ca. 6640 cm^{-1} [31, 32]). In the C_2 local crystal field symmetry, 16-fold degeneracy of the free ion is partly removed by splitting the ground multiplet into eight Kramers doublets. From spectroscopic data [31] for the $KGd(WO_4)_2$ single crystal doped with Er^{3+}, the energy intervals Δ_i ($i = 1, 2, \ldots, 7$) between the ground doublet and other doublets were determined. They are equal to 50.4, 110.8, 182.7, 243.2, 395.7, 493.5 and 519.4 K, respectively, at temperature $T = 5$ K. It was also determined that these intervals are temperature independent up to room temperature. Since the temperature dependences of magnetization were measured over a temperature range of 4–150 K, it was necessary to take into account in calculations the presence of, at least, the next two lowest doublets. Using the Landé factor for Er^{3+}, $g_J = 6/5$, the maximal value of the spectroscopy splitting factor for the ground doublet was found to be

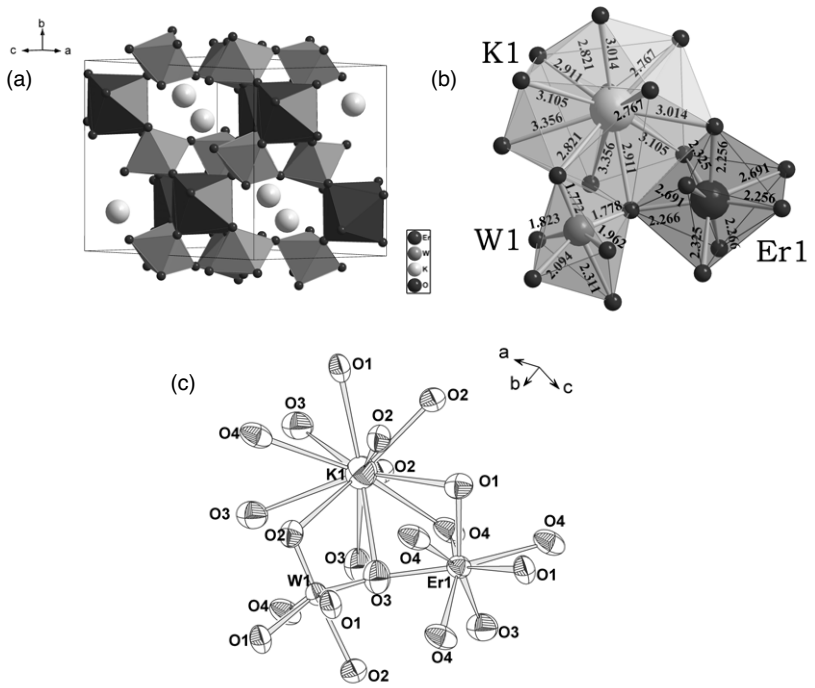

Figure 1. (a) Unit cell of $KEr(WO_4)_2$ with W and Er polyhedra. (b) Er, K and W polyhedra with marked distances to ligands. (c) Thermal ellipsoids with probability factor equal to 99% [22].

equal to $g_{\max} = 18$. For simplicity, the crystal field Hamiltonian was assumed to have axial symmetry:

$$\hat{H} = 3D_0(\hat{J}_z^2 - J^2) - \mu_B g_J \hat{J}_z H_z \tag{1}$$

where $D_0 = -1.199$ K, $J = 15/2$, J_z is the z-projection of the total angular momentum, and μ_B is the Bohr magneton. From equation (1) we find that the energy interval between the ground and the first excited doublet is equal to 50.4 K and that between the ground and the second excited doublet has the value of 93.5 K, that does not differ strongly from the experimental value of 110.8 K. One can point out that (1) is a model Hamiltonian which can be used only to determine susceptibility at temperatures below 100 K.

4.2. Magnetic susceptibility near the magnetic phase transition

Figure 2 shows the temperature dependence of the ac susceptibility of $KEr(WO_4)_2$ measured near the phase transition. The main peculiarity of the $\chi(T)$ dependence is the presence of the anomaly peaking at $T_1 = 0.48$ K, which is similar to the behaviour of the phase transition to the antiferromagnetic state in dysprosium double tungstates near the MPT transition [15–17]. The absence of a sharp peak and the anomaly broadening at T_1 allows us to suppose that this transition is a second-order one. The presence of an inflection point on $\chi(T)$ above the transition temperature (near 0.8 K) can be attributed to both the low-dimensional character of the magnetic ordering and the short-range ordering effects. Also, we do not exclude the possibility of crossover from 2D Ising to low-dimensional Heisenberg models at lowering of temperature. This assumption is supported by the specific heat data (see below).

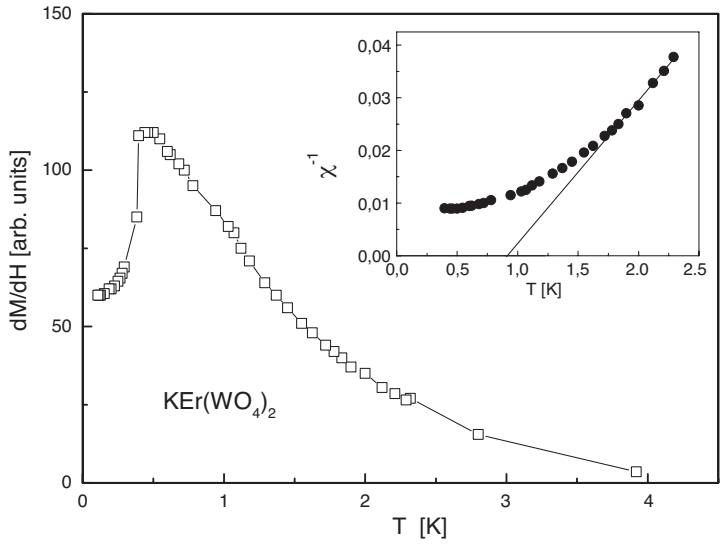

Figure 2. Temperature dependence of ac susceptibility near the magnetic phase transition. Inset—inverse susceptibility as a function of temperature.

Table 4. Calculated values of susceptibility, g-factors and paramagnetic temperature.

	$H = 1$ kOe (a_1c_1)		$H = 1$ kOe (a_1b_1)	
Parameters	M_x	M_z	M_{a1}	M_{b1}
Susceptibility χ_0 (emu mol^{-1})	0.013 03	−0.003 49	−0.1092	−0.229
First factor g_1	4.54	17.38	18.09	12.84
Second factor g_2	12.36	0.341	12.695	21.69
Paramagnetic temperature θ (K)	1.141	−0.957	−3.863	0.173
Mean square root deviation (%)	0.065	0.076	0.42	1.1
Temperature interval of fitting (K)	28–172	28–191	11–60	8–61

The temperature dependence of the reciprocal susceptibility, $1/\chi(T)$ (inset to figure 2), is used for rough estimation of the paramagnetic Curie temperature θ_i in the temperature interval of 1.7–2.3 K in accordance with the Curie–Weiss law, $\chi_i = C_i/(T - \theta_i)$, where $C_i = N_A(\mu_B g_i)^2 S(S+1)/3k$, N_A is the Avogadro's number, $S = 1/2$ the effective spin for the lowest doublet and k the Boltzmann's constant. Since the measurements were performed on the elongated sample with a small demagnetizing factor, the point of intersection of the $1/\chi(T)$ curve with the temperature axis determines the paramagnetic Curie temperature θ. The found θ value is equal to $+0.915$ K, which is close to the value θ_x obtained from magnetization (table 4).

The low value of the magnetic phase transition temperature reveals a small value of exchange interactions between Er^{3+} ions. Thus, one can suppose that the dipole–dipole contribution to spin–spin interactions, which determine the magnetic properties of $KEr(WO_4)_2$, is comparable with the superexchange contribution. The positive sign of the paramagnetic Curie temperature testifies to the ferromagnetic character of the exchange interaction along the x axis. To estimate the competition between antiferromagnetic interactions along the z axis and ferromagnetic interactions along the x axis we calculated the total energy of possible magnetic structures (see the next section).

4.3. Parameters of magnetic interactions

To determine the magnetic interaction parameters it is necessary to add to Hamiltonian (1) the magnetic dipole and exchange interactions. For the anisotropic Heisenberg model in the mean field approximation this requirement is equivalent to substitution in equation (1) of the H value by the effective field $\tilde{H}$:

$$\tilde{H}_z = H_z + \frac{2\tilde{J}_z(0)}{\mu_B g_z}\langle S^z\rangle, \tag{2}$$

where $\tilde{J}_z(0) = z\tilde{J}_z$, z and $\tilde{J}_z$ are the number of nearest neighbours and the parameter of pair exchange, respectively.

In figures 3(a) and (b) the experimental (points) and fitted (lines) temperature dependences of $1/\chi(T) = H/M$, where M is the magnetization in the $a_I b_I$ and $a_I c_I$ planes, are shown. In figure 3(a), the full square and open circles correspond to maximum and minimum values of reciprocal susceptibility in the $a_I c_I$ plane, respectively. First of all we call attention to the fact that the upper curve of $1/\chi(T)$ has a large value of the paramagnetic Curie temperature. This peculiarity can be explained by the influence of the first excited Kramers doublet. Then, using the Hamiltonian (1) and equation (2), it is easy to write the expression for molar susceptibility:

$$\chi_i(T) = \frac{\mu_B^2 N_A}{k_B}\frac{f_i(T)}{T - \frac{4\theta_i}{15g_J^2}f_i(T)} \tag{3}$$

where $f_i(T) = \frac{g_i^2+g_{1i}^2\exp(-42D_0/T)}{4(1+\exp(-42D_0/T))}$ is the contribution of the crystal field to the susceptibility, g_i and g_{1i} are the g-factors of the ground and first excited doublets in the ith direction, N_A is the Avogadro constant and $\theta_i = \frac{2S(S+1)\tilde{J}_i(0)}{3k_B}$. In table 4 the parameters found are presented.

According to EPR data [33], the **z** axis is deflected from the $\mathbf{a_I}$ axis in the $a_I c_I$ plane by the angle 126°. The maximal magnetization obtained from an angular dependence of magnetization in the $a_I c_I$ plane is observed at the angle close to the value determined by EPR. In further calculations the values $g_z = 17.38$, $g_x = 4.54$, $g_b = 12.84$, $\theta_z = -0.957$ K, $\theta_x = 1.141$ K and $\theta_b = 0.173$ K were used. The negative sign of the paramagnetic Curie temperature along the **z** direction reflects an antiferromagnetic character of interactions between Er ions.

In order to find the magnetic structure and value of exchange interactions, one should transform the g-tensor to the coordinate system connected with the basic crystallographic directions, $\mathbf{a_I}$, $\mathbf{b_I}$, and $\mathbf{c_I}$. Let us consider the Hamiltonian:

$$\hat{H} = -\mu_B\{g_z\tilde{H}_z S^z + g_x\tilde{H}_x S^x\}, \tag{4}$$

where the effective field along the ith direction is determined according to equation (2). If the external field H is directed at an angle ξ in relation to the **z** axis, its components are

$$H_x = -H\sin(\xi), \qquad H_z = H\cos(\xi). \tag{5}$$

To find eigenvalues of the Hamiltonian, it is necessary to transform it unitarily by rotation around the **y** axis by an α angle to the coordinate system connected with mean magnetization $\langle\tilde{S}\rangle$. In this case spin components will be transformed as follows:

$$S^x = \tilde{S}^x\cos(\alpha) - \tilde{S}^z\sin(\alpha), \qquad S^z = \tilde{S}^x\sin(\alpha) + \tilde{S}^z\cos(\alpha). \tag{6}$$

Substituting equation (6) in (4), taking into account that according to equation (6)

$$\langle S^x\rangle = -\langle\tilde{S}\rangle\sin\alpha, \qquad \langle S^z\rangle = -\langle\tilde{S}\rangle\cos\alpha, \tag{7}$$

and comparing the nondiagonal component of equation (4) to zero, one can obtain the equation determining the angle α. The expectation value of the spin $\langle\tilde{S}\rangle$ can be expressed as the

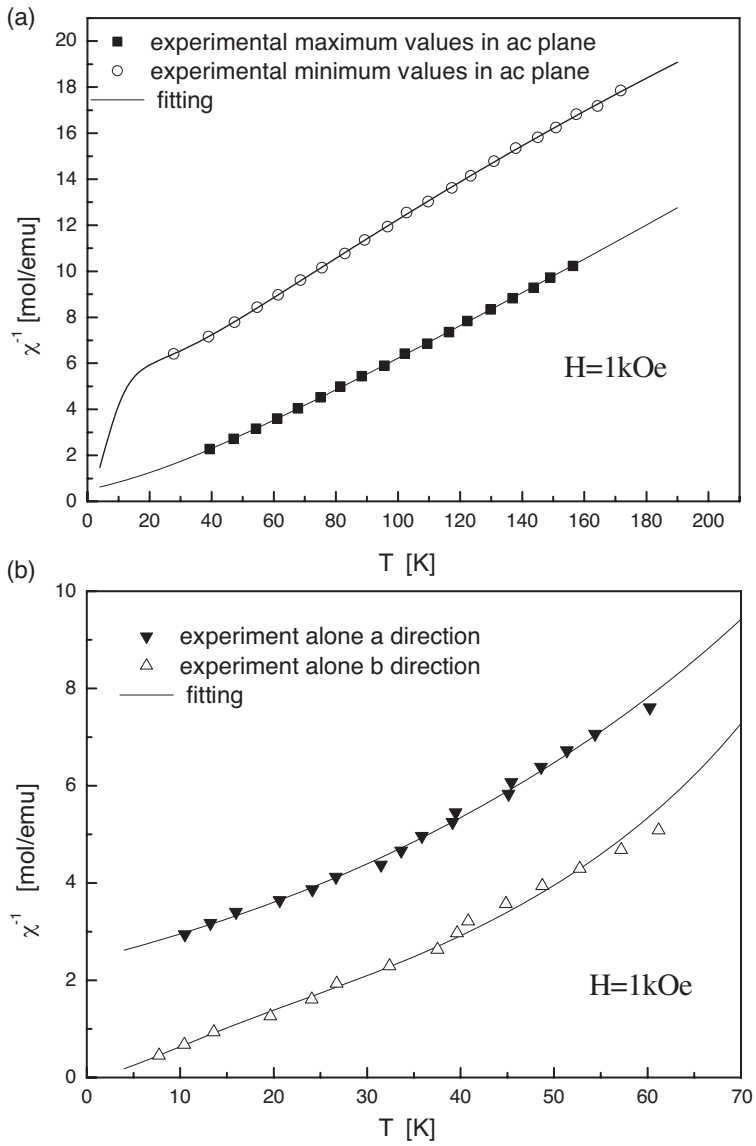

Figure 3. Experimental (points) and fitted curves (lines) of reciprocal susceptibility: (a) in the $a_I c_I$ plane (full square and open circles correspond to maximum and minimum values of susceptibility, respectively); (b) along the $\mathbf{a_I}$ and $\mathbf{b_I}$ directions (full and open triangles, respectively) at $H = 1$ kOe.

following function of α:

$$\langle \tilde{S} \rangle = \frac{\mu_B H \{g_z \cos(\xi) \sin(\alpha) - g_x \sin(\xi) \cos(\alpha)\}}{\sin(2\alpha)\{\tilde{J}_x(0) - \tilde{J}_z(0)\}}. \tag{8}$$

The effective field $\tilde{H}$ in the coordinate system where the mean spin is parallel to the $\mathbf{z}$ axis has a form

$$\tilde{H} = H \left\{ \frac{\tilde{J}_x}{\tilde{J}_x - \tilde{J}_z} \frac{g_\parallel}{\cos(\alpha)} - \frac{\tilde{J}_z}{\tilde{J}_x - \tilde{J}_z} \frac{g_\perp}{\sin(\alpha)} \right\}, \tag{9}$$

where $g_{\parallel} = g_z \cos(\xi)$, $g_{\perp} = g_x \sin(\xi)$. Substituting equations (8) and (9) in the self-consistent equation for mean spin

$$\langle \tilde{S} \rangle = \frac{1}{2} \tanh\left(\frac{\mu_B \tilde{H}}{2k_B T}\right), \tag{10}$$

a transcendental equation for α is obtained. For angles $\alpha \neq 0, \pi/2$, when the H field deviates from the **z** and **x** directions, this equation can be easily solved numerically. The obtained solutions of equation (10) were used for both calculation of magnetization

$$M(\xi, H) = \mu_B g N \langle \tilde{S} \rangle \cos\xi \cos\alpha(1 + \tan(\alpha)\tan(\xi)), \tag{11}$$

where $g = \sqrt{g_{\parallel}^2 + g_{\perp}^2}$, and for comparison with the experimental field dependence of magnetization for different directions of external magnetic field in the xz plane. Using equations (8)–(10) in the high-temperature approximation when $\mu_B H/(k_B T) \ll 1$ we obtain the Curie–Weiss law for susceptibility χ in the form

$$\chi(T, \xi) = \frac{C(\xi)}{T - \theta_{\xi}} \tag{12}$$

where the Curie constant along the field direction is given by the formula

$$C(\xi) = \frac{1}{4k_B} \mu_B^2 g \tilde{g} N,$$

and

$$\tilde{g} = g_{\parallel} \cos(\xi) + g_{\perp} \sin(\xi) \tag{13}$$

and paramagnetic temperature θ_{ξ} is transformed in the following manner:

$$\theta_{\xi} = \frac{1}{\tilde{g}} \{\theta_z g_{\parallel} \cos(\xi) + \theta_x g_{\perp} \sin(\xi)\}. \tag{14}$$

Here, θ_z and θ_x are the paramagnetic temperatures along the **z** and **x** axes, respectively. Apparently, in the low-temperature region ($T \ll 50$ K) we may neglect the influence of the upper doublet.

To determine the possible magnetic structure the g-factors and paramagnetic temperature values along the $\mathbf{a_I}$, $\mathbf{b_I}$ and $\mathbf{c_I}$ crystallographic directions should be known. The latter are easily found using equations (13) and (14) and knowing the rotation angles of the magnetic axes relative to the appropriate directions. Because of a weak distortion of orthorhombic structure the angle between the $\mathbf{a_I}$ and $\mathbf{c_I}$ axes differs slightly from 90°. However, it has no high significance since we will take the average rotation angles of the magnetic axes relative to the appropriate $\mathbf{a_I}$ and $\mathbf{c_I}$ axes. The paramagnetic temperature and g-factor values along the main directions calculated are presented in table 5. Using equations (8)–(11) and the values of θ_z, θ_x, g_z and g_x, the field dependences of magnetization, $M(H)$, for various rotation angles of an external field, ξ, in relation to the **z** axis were plotted (figure 4). Unfortunately, the parameters θ_i and g (see the appropriate columns with the designation 'High T' in table 5) obtained from the analysis of high-temperature susceptibility give a susceptibility value at $T = 4.2$ K different from the value obtained from an initial slope of the experimental $M(H)$ dependence at $\xi = 0°$ (**z** axis) and $\xi = 90°$ (**x** axis). Some variation of the calculated parameters was carried out to achieve the best agreement between theory and experiment in the low-temperature region. The adjusted values are given in columns with the designation 'Low T' in table 5. The values of magnetization were corrected taking into account a weak diamagnetic susceptibility, $\chi_0 = -0.000\,32$ emu g^{-1}. Its contribution is essential for a small magnetization value along the **x** axis. In figure 4, the calculated (line) and experimental (point) $M(H)$ dependences are

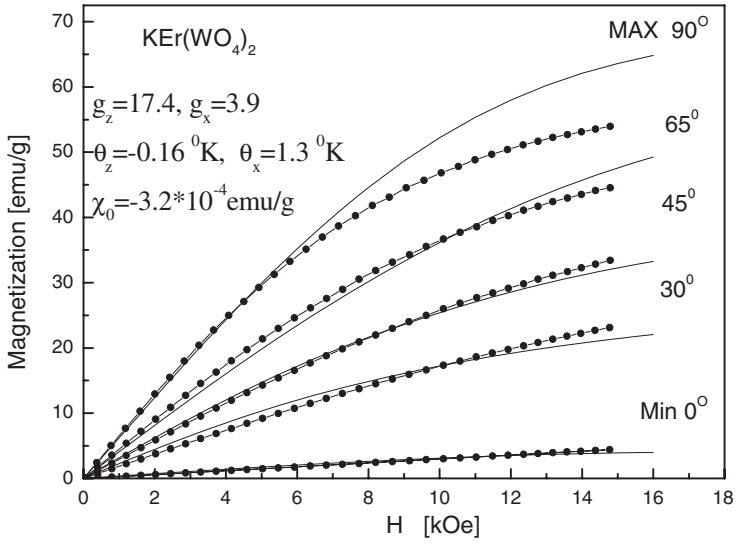

Figure 4. Experimental (points) and calculated (lines) field dependences of magnetization in the xz plane for different angles, ξ, between the direction of the magnetic field and the **z** axis.

Table 5. Parameters of magnetic interactions.

	g-factor		Paramagnetic temperature θ (K)		Parameter of pair exchange from structure (K)	Dipole contribution in θ from demagnetization and Lorentz sphere (K)	Dipole contribution in θ inside Lorentz sphere (K)	Energy of ground magnetic state (K)
Direction	High T	Low T	High T	Low T				
z	17.38	17.38	−0.957	−0.16	—	—	—	—
x	4.54	3.9	1.141	1.3	—	—	—	—
a	10.96	10.64	−0.521	0.109	−0.344 (−0.659)	0.47	1.811	−2.963
b	12.84	10.98	0.173	0.173	−0.287 (−0.622)	0.5	1.565	−3.133
c	10.53	10.19	−0.475	0.138	0.692 (0.403)	−0.867	−3.008	−6.137

shown for ξ values equal to 0°, 25°, 45°, 60° and 90° at temperature $T = 4.2$ K. A reasonable agreement between theory and experiment is observed. There is some difference in values of magnetization saturation at $\xi = 0°$ that is indicative of a certain error in g-factor values calculated.

For analysis of possible magnetic structure realized at phase transition we have used the g and θ_i parameters in the 'Low T' columns (table 5). All calculations were carried out in the coordinate system connected with the crystallographic $\mathbf{a_I}$, $\mathbf{b_I}$ and $\mathbf{c_I}$ axes. Since the exchange parameter and ordering temperature are sufficiently small it is necessary to take into account the magnetic dipole interactions.

In the first approximation the orthorhombic Bravais lattice is considered in which all magnetic ions are equivalent. The ground state energy was estimated taking into account the dipole and exchange interactions and using the method in [34]. The Lorentz sphere was taken with a diameter of ∼260 Å. The dipole sums and their contribution to paramagnetic

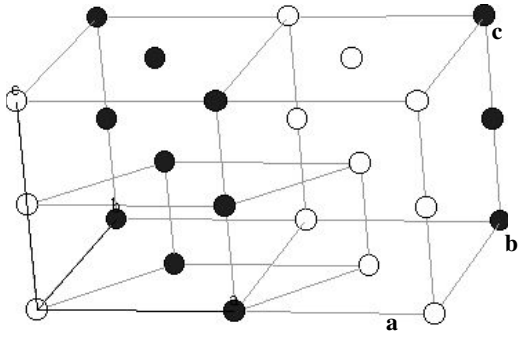

Figure 5. Magnetic structure of ground state of $KEr(WO_4)_2$ calculated taking into account exchange and dipolar interactions (solid and open circles correspond to opposite directions of spins along the **z** axis).

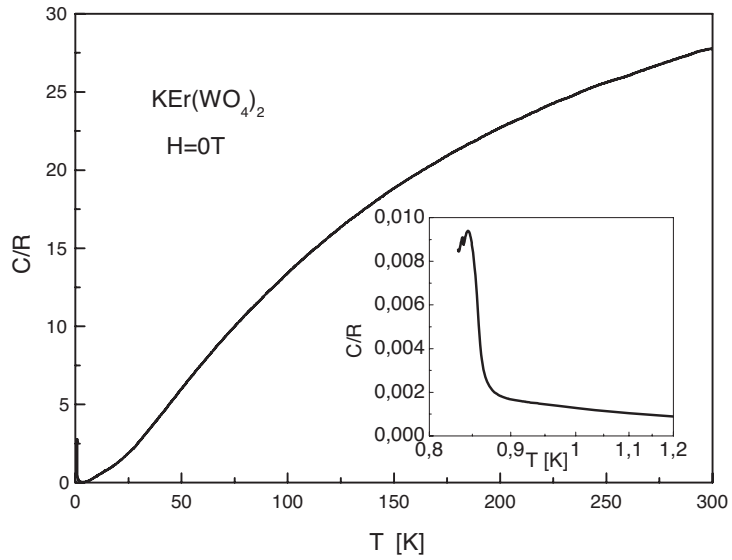

Figure 6. Experimental temperature dependence of specific heat. Inset: temperature dependence of the specific heat at 1.2–0.82 K is shown.

temperature both inside and outside the Lorentz sphere were calculated. This allowed us to find the exchange interaction parameters along the main crystallographic direction (sixth column of table 5; in brackets an effective exchange with the Lorentz term is given). The last column gives the minimal energies for directions of mean spin $\langle\tilde{S}\rangle$ along the $\mathbf{a_I}$, $\mathbf{b_I}$ and $\mathbf{c_I}$ axes. Minimal energy of $E_c = -6.137$ K with spin $\langle\tilde{S}\rangle$ directed along the $\mathbf{c_I}$ axis corresponds to a ferromagnetic plane which is ordered antiferromagnetically and passes through one of the long diagonals of the parallelepiped (figure 5). In table 5, for comparison we give the energy values for the $\mathbf{a_I}$ and $\mathbf{b_I}$ directions, which are essentially large.

4.4. Magnetic specific heat

In figure 6, the experimental temperature dependence of specific heat, C/R, where R is the gas constant, is presented for the temperature interval from 0.8 to 300 K. Below $T_2 = 0.85$ K (inset

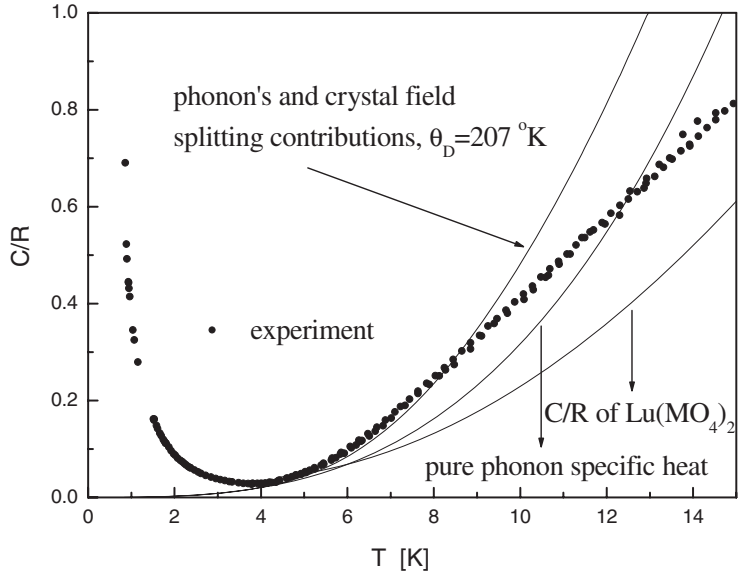

Figure 7. Calculated crystal and phonon contributions in specific heat (lines) in temperature intervals from 0.9 to 14 K. Circles—experimental points.

to figure 6), an abrupt fall of specific heat is observed. At this temperature the susceptibility has a visible break (figure 2).

In the low-temperature region, the most interesting for the present studies, the measured specific heat is a sum of magnetic, Schottky and lattice contributions. Since the real phonon spectrum for $KEr(WO_4)_2$ is not known, it is not possible to calculate the actual phonon contribution to the specific heat. It was assumed that over the temperature range from 0.8 to 10 K the Debye model gives an adequate description of the phonon specific heat. To determine the Debye temperature, it was assumed that the magnetic contribution can be neglected above 5 K. Taking into account that the magnetic transition occurs at $T_1 = 0.48$ K, this assumption seems to be well based. Next, the Schottky contribution has been calculated according to the formula

$$\frac{C_{\mathrm{Sch}}T^2}{R} = \frac{\sum_{i=1}^{7}\Delta_i^2\exp(-\Delta_i/T)}{1+\sum_{i=1}^{7}\exp(-\Delta_i/T)} - \left[\frac{\sum_{i=1}^{7}\Delta_i\exp(-\Delta_i/T)}{1+\sum_{i=1}^{7}\exp(-\Delta_i/T)}\right]^2 \tag{15}$$

into which Δ_i values are determined with spectroscopic studies [24, 25]. By subtracting the calculated Schottky contribution, C_{Sch}/R, (equation (15)) from the measured specific heat, the lattice contribution has been obtained. The Debye temperature, $T_{\mathrm{D}} = 207$ K, has been determined by fitting the Debye function,

$$C_{\mathrm{D}}/R = 108\left(\frac{T}{T_{\mathrm{D}}}\right)^3\int_0^{T_{\mathrm{D}}/T}\frac{x^4\exp(x)}{(\exp(x)-1)^2}\,\mathrm{d}x, \tag{16}$$

to the points obtained for the temperature range from 5.1 to 9.5 K. Here x is the inner variable. In figure 7, the measured total specific heat, as well as the phonon and Schottky contributions, are shown. For comparison, a similar curve for nonmagnetic lutetium molybdate is also presented.

Extracting this total contribution from experimental values C/R, the magnetic specific heat was found (figure 8, solid circles). For comparison the total specific heat is plotted by

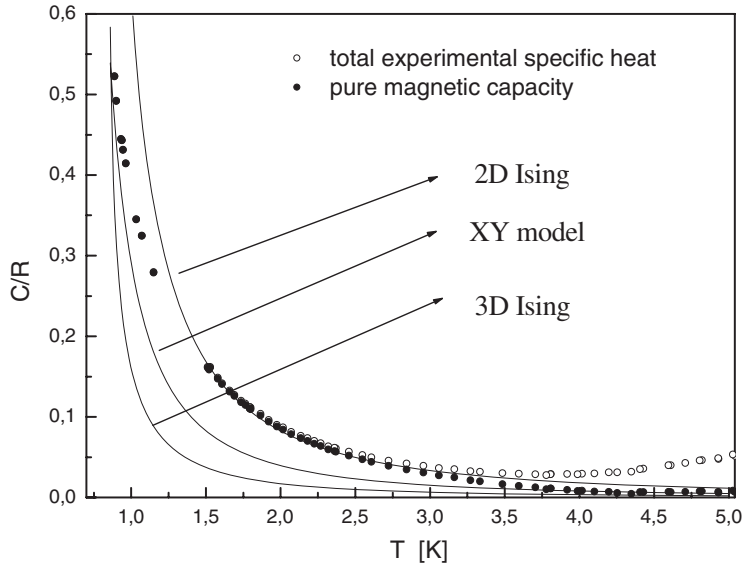

Figure 8. Magnetic contribution (full circles) to total specific heat (open circles) and calculated (lines) magnetic specific heat for 2D Ising, 3D Ising and XY model.

open circles. To compare the experimental data with theoretical predictions, the temperature dependences of specific heat in the framework of 2D, 3D and XY models were calculated.

To estimate an effective exchange parameter we used both the temperature T_1 of the ac-susceptibility cusp (figure 2) and the temperature T_2 of the specific heat maximum (inset to figure 6). Using the Ising relation between T_i and the AFM pair exchange parameter $\tilde{J}$

$$\tilde{J} = T_i \ln(\sqrt{2} - 1), \tag{17}$$

the pair exchange parameter $\tilde{J}_1 = -0.423$ K was obtained for $T_i = T_1$. Unfortunately, use of the T_1 temperature does not allow us to fit the experimental and theoretical $C/R(T)$ dependence in a framework of the low-dimensional Ising model at low temperatures. Using $T_2 = 0.85$ K in equation (17) we found the exchange parameter $\tilde{J} = -0.764$ K. This value characterizes an effective exchange in the low-dimensional Ising model and is very close to the values of $\tilde{J} \sim -0.6$–0.7 K (sixth column of table 5) obtained from the analysis of magnetic structure for $\mathbf{a_I}$ and $\mathbf{b_I}$ directions taking into account the dipole–dipole contribution. Using the $\tilde{J}_2$ value we calculated a specific heat in the framework of the 2D Ising model (figure 8). In figure 8, the calculated temperature dependences of specific heat for 3D Ising and XY models [35, 36] using the T_2 value are also presented. The best agreement with the experimental data is observed for the 2D Ising model from 5 K down to 1.5 K. At lower temperatures, a crossover to a 3D Ising and XY magnetic behaviour is not excluded. However, this question needs further more detailed investigation.

Summarizing, theoretical results obtained in the frame of the 2D Ising model are consistent with experimental data. This can be considered evidence of the existence in the studied compound of a low-dimensional character of magnetic ordering with ferromagnetic magnetic moment along the $\mathbf{c_I}$ axis. The correlation of the $\tilde{J}_2$ and $\tilde{J}_3$ parameter exchange calculated in mean field approximations taking into account the fluctuations may be confirmation of the inferred magnetic structure obtained.

Acknowledgments

This work was supported by EU project DT-CRYS, NMP3-CT-2003-505580, by the Polish State Committee on Science (KBN) (decision of project No. 72/E-67/SPB/6. PR/DIE 430/2004-2006).

References

[1] Griebner U, Liu J, Rivier S, Aznar A, Grunwald R, Sole R M, Aguilo M, Diaz F and Petrov V 2005 *IEEE J. Quantum Electron.* **41** 408
Mateos X, Petrov V, Aguilo M, Sole R M, Gavalda J, Massons J, Diaz F and Griebner U 2004 *IEEE J. Quantum Electron.* **40** 1056
Petrov V, Güell F, Massons J, Gavalda J, Sole R M, Aguilo M, Diaz F and Griebner U 2004 *IEEE J. Quantum Electron.* **40** 1244
Kaminiski A A 1996 *Crystalline Laser, Physical Processes and Operating Schemes* (London: CRC Press) p 499
Hellstrom J E, Bjurshagen S, Pasiskevicius V, Liu J, Petrov V and Griebner U 2006 *Appl. Phys.* B **83** 235
Romanyuk Y E, Borca C N, Pollnau M, Rivier S, Petrov V and Griebner U 2006 *Opt. Lett.* **31** 53
Griebner U, Rivier S, Petrov V, Zorn M, Erbert G, Weyers M, Mateos X, Massons A J and Diaz F 2005 *Opt. Express* **13** 3465
Rivier S, Mateos X, Petrov V, Griebner U, Aznar A, Silvestre O, Sole R, Aguilo M, Diaz F, Zorn M and Weyers M 2005 *Opt. Lett.* **30** 2484
Kato A, Oishi S, Shishido T, Yamazaki M and Iida S 2005 *J. Phys. Chem. Solids* **66** 2079
Kumaran A S, Chandru A L, Babu S M, Bhaumik I, Ganesamoorthy S, Karnal A K, Wadhawan V K and Ichimura M 2005 *J. Cryst. Growth* **275** e2117
Mateos X, Pujol M C, Guell F, Galan M, Sole R M, Gavalda J, Aguilo M, Massons J and Diaz F 2004 *IEEE J. Quantum Electron.* **40** 759
[2] Borowiec M T, Prokhorov A D, Krygin I M, Dyakonov V P, Wozniak K, Dobrzycki L, Zayarnyuk T, Baranski M, Domuchovski W and Szymczak H 2006 *Physica* B **371** 205
Borowiec M T, Prochorov A A, Prochorov A D, Dyakonov V P and Szymczak H 2003 *J. Phys.: Condens. Matter* **15** 5113
Khatsko E N, Cherny A S, Rykova A I, Borowiec M T, Szymczak H and Dyakonov V P 2003 *Low Temp. Phys.* **29** 1328
Kovacs L, Borowiec M T, Majchrowski A, Baraldi A and Capelletti R 2005 *Cryst. Res. Technol.* **40** 444
[3] Diaz F, Mateos X, Sole R, Gavalda J, Aguilo M and Massons J 2006 *Opt. Mater.* **28** 423
Rico M, Liu J, Griebner U, Petrov V, Serrano M D, Esteban B F, Cascales C and Zaldo C 2004 *Opt. Express* **12** 5362
Major A, Nikolakakos I, Aitchison J S, Ferguson A I, Langford N and Smith P W E 2003 *Appl. Phys.* B **77** 433
[4] Dergachev K G, Kobets M I, Aloginov A and Khatsko E N 2006 *Low Temp. Phys.* **31** 862
Aloginov A, Khatsko E N, Cherny A S, Baumer B N, Rykova A I, Kalinin P S and Sulpis A 2006 *Low Temp. Phys.* **32** 68
[5] Kunpeng W, Jianxiu Z, Jiyang W, Huaijin Z, Zhengping W, Wentao Y, Xuping W, Qingming L, Mingfang B and Boughton R I 2005 *J. Appl. Phys.* **98** 46101
Jianxiu Z, Kunpeng W, Jiyang W, Huaijin Z, Wentao Y, Xuping W, Zhengping W, Qingming L, Mingfang B, Ran D G, Ling Z C and amd Xia H R 2005 *Appl. Phys. Lett.* **87** 61104
Biswal S, O'Connor S P and Bowman S R 2005 *Appl. Opt.* **44** 3093
[6] Abragam A and Bleaney B 1970 *Electron Paramagnetic Resonance of Transition Ions* vol 1 (Oxford: Clarendon)
Taylor K N R and Darby M I 1972 *Physics of Rare Earth Solids* (London: Chapman and Hall)
[7] Borowiec M T, Watterich A, Zayarnyuk T, Dyakonov V P, Majchrowski A, Zmija J, Baranski M and Szymczak H 2004 *J. Appl. Spectrosc.* **71** 888
[8] Kaplan M D and Vekhter B G 1995 *Cooperative Phenomena in Jahn–Teller Crystals* (New York: Plenum)
Gehring G A and Gehring K A 1974 *Rep. Prog. Phys.* **38** 1
[9] Krynetskii I B, Popkov A F, Popov A I, Borowiec M T, Nabialek A, Zayarnyuk T and Szymczak H 2006 *Phys. Solid State* **48** 1467
Borowiec M T, Krynetski I, Dyakonov V P, Nabiaek A, Zayarnyuk T and Szymczak H 2006 *New J. Phys.* **8** 124
[10] Pelikh L N and Gurskas A A 1979 *Fiz. Tverd. Tela* **21** 1223
[11] Skorobogatova I V and Savchenko E M 1980 *J. Low Temp. Phys.* **6** 240

[12] Borowiec M T, Dyakonov V P, Kamenev V, Nabialek A, Prokhorov A D, Szymczak H and Zaleski M 1998 *Acta Phys. Pol.* A **94** 71
[13] Szewczyk A, Gutowska M P, Piotrowski K, Gutowski M, Borowiec M T, Dyakonov V, Szymczak H and Gladczuk L 1998 *J. Phys.: Condens. Matter* **10** 10539
[14] Dyakonov V, Markovich V, Kovarskii V, Markovich A, Borowiec M T, Jedrzejczak A and Szymczak H 1998 *Fiz. Tverd. Tela* **40** 750
[15] Borowiec M T, Dyakonov V, Jedrzejczak A, Markovich V, Pavlyuk A, Szymczak H, Zubov E and Zaleski M 1998 *J. Low Temp. Phys.* **110** 1003
[16] Borowiec M T, Dyakonov V, Jedrzejczak A, Markovich V, Pavlyuk A, Szymczak H, Zubov E and Zaleski M 1998 *Phys. Lett.* A **243** 85
[17] Khatsko E N, Cherny A S, Rykova A I, Borowiec M T, Szymczak H and Dyakonov V P 2003 *Low Temp. Phys.* **29** 1328
Borowiec M T, Dyakonov V, Fita I, Nabialek A, Pavlyuk A, Szewczyk A, Szymczak H, Zaleski M and Zubov E 1999 *J. Magn. Magn. Mater.* **95** 119
[18] Kumaran A S, Chandru A L, Babu S M and Ichimura M 2005 *J. Cryst. Growth* **275** e1901
[19] Kaminski A A, Konstantinova A F, Orekhova V P, Butashin A F, Klevtsova R F and Pavlyuk A A 2001 *Crystallogr. Rep.* **46** 665
[20] Kaminski A A, Bagaev S N and Pavlyuk A A 1995 *Phys. Status Solidi* a **151** K53
[21] Pujol M C, Massons J, Aguilo M, Diaz F, Rico M and Zaldo C 2002 *IEEE J. Quantum Electron.* **38** 93
[22] Pujol M C, Barsukova M A, Guell F, Mateos X, Sole R, Gavalda J, Massons J, Diaz F, Klopp P, Griegner U and Petrov V 2002 *Phys. Rev.* B **65** 165121
[23] Majchrowski A, Borowiec M T and Michalski E 2004 *J. Cryst. Growth* **264** 201
[24] Majchrowski A 1999 *Proc. SPIE* **3724** 18
[25] Kirshbaum K, Martin A and Pinkerton A 1997 *J. Appl. Crystallogr.* **30** 514
[26] Sheldrick G M 1990 *Acta Crystallogr.* A **46** 467
[27] Sheldrick G M *SHELXL93: Program for the Refinement of Crystal Structures* University of Göttingen, Germany
[28] Wilson A J C (ed) 1992 *International Tables for Crystallography* vol C (Dordrecht: Kluwer–Academic)
[29] Pujol M C, Mateos X, Sole R, Massons J, Gavalda J, Diaz F and Aguilo M 2001 *Mater. Sci. Forum* **378–381** 710
Klevtsov P V and Kozeeva L P 1969 *Sov. Phys.* **14** 187
Pujol M C, Sole R, Massons J, Gavald J, Solans X, Zaldo C, Diaz F and Aguilo M 2001 *J. Appl. Crystallogr.* **34** 1
Pujol M C, Mateos X, Sole R, Massons J, Gavalda J, Solans X, Diaz F and Aguilo M 2002 *J. Appl. Crystallogr.* **35** 108
[30] Hahn Th (ed) 1983 *The International Tables for Crystallography* vol A (Dordrecht: Reidel) p 185
[31] Mateos X, Pujol M C, Guell F, Galan M, Sole R, Gavalda J, Aguilo M, Massons J and Diaz F 2004 *IEEE J. Quantum Electron.* **40** 759
Pujol M C, Rico M, Zaldo C, Sole R, Nikolov V, Solans X, Aguilo M and Diaz F 1999 *Appl. Phys.* B **68** 187
[32] Borowiec M T, Kharchenko Y M, Zayarnyuk T, Dyakonov V P, Baranski M and Szymczak H 2004 *J. Appl. Spectrosc.* **71** 651
[33] Borowiec M T, Prokhorov A A, Dyakonov V P, Prokhorov A D and Szymczak H 2003 *J. Phys.: Condens. Matter* **15** 5113
[34] Niemeyer T H 1972 *Physica* **57** 281
[35] Sykes M F, Hunter D L, McKenzie D S and Heap B R 1972 *J. Phys. A: Math. Gen.* **5** 667
[36] Betts D D 1974 *Phase Transition and Critical Phenomena* vol 3, ed C Domb and M S Green (New York: Academic) p 569